Acta Crystallographica Section D
Biological Crystallography
ISSN 0907-4449

Structure of a double-stranded DNA (6–4) photoproduct in complex with the 64M-5 antibody Fab

Hideshi Yokoyama,[a]* Ryuta Mizutani[b] and Yoshinori Satow[c]

[a]School of Pharmaceutical Sciences, University of Shizuoka, Japan, [b]Department of Applied Biochemistry, School of Engineering, Tokai University, Japan, and [c]Graduate School of Pharmaceutical Sciences, University of Tokyo, Japan

Correspondence e-mail: h-yokoya@u-shizuoka-ken.ac.jp

Received 17 October 2012
Accepted 6 December 2012

PDB Reference: 64M-5 Fab complexed with a double-stranded DNA (6–4) photoproduct, 3vw3

DNA photoproducts with (6–4) pyrimidine–pyrimidone adducts formed by ultraviolet radiation have been implicated in mutagenesis and cancer. The crystal structure of double-stranded DNA containing the (6–4) photoproduct in complex with the anti-(6–4)-photoproduct antibody 64M-5 Fab was determined at 2.5 Å resolution. The T(6–4)T segment and the 5′-side adjacent adenosine are flipped out of the duplex and are accommodated in the concave antigen-binding pocket composed of six complementarity-determining regions (CDRs). A loop comprised of CDR L1 residues is inserted between the flipped-out T(6–4)T segment and the complementary DNA. The separation of strands by the insertion of the loop facilitates extensive and specific recognition of the photoproduct. The DNA helices flanking the T(6–4)T segment are kinked by 87°. The 64M-5 Fab recognizes the T(6–4)T segment dissociated from the complementary strand, indicating that the (6–4) photoproduct can be detected in double-stranded DNA as well as in single-stranded DNA using the 64M-5 antibody. The structure and recognition mode of the 64M-5 antibody were compared with those of the DNA (6–4) photolyase and nucleotide-excision repair protein DDB1–DDB2. These proteins have distinctive binding-site structures that are appropriate for their functions, and the flipping out of the photolesion and the kinking of the DNA are common to mutagenic (6–4) photoproducts recognized by proteins.

1. Introduction

DNA photoproducts produced by ultraviolet radiation induce mutations, cellular transformation and cell death (Lindahl, 1993). Pyrimidine (6–4) pyrimidone DNA photoproducts (Fig. 1) are produced as often as cyclobutane pyrimidine dimers, but are approximately tenfold more mutagenic (LeClerc *et al.*, 1991).

For detection and quantification of the (6–4) photoproduct, a series of monoclonal antibodies, 64M-2, 64M-3 and 64M-5, were simultaneously established from BALB/c mice immunized with ultraviolet-irradiated single-stranded calf thymus DNA (Mori *et al.*, 1991). These antibodies are highly specific for the (6–4) photoproduct and show no affinity for other damaged or undamaged DNA (Kobayashi *et al.*, 1998). In crystal structures of the (6–4) DNA photoproduct in complex with the 64M-2 Fab fragment, the T(6–4)T segment is in a closed circular form and the base planes covalently linked by the C6—C4 bond are nearly perpendicular (Yokoyama *et al.*, 2000, 2012). The crystal structure revealed that the specific recognition by the 64M-2 antibody is ascribable to the structural environment of the binding-site pocket composed of His27dL, Tyr32L, Leu93L, Trp33H, Ser58H, Arg95H and Tyr100iH (light-chain and heavy-chain residues are numbered

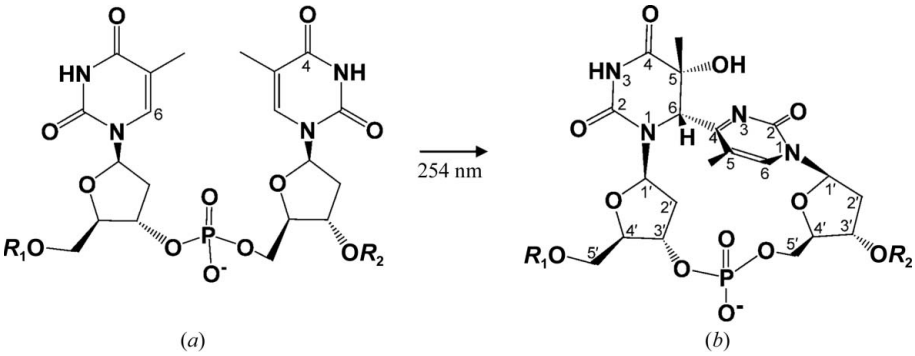

Figure 1
A DNA (6–4) photoproduct formed by ultraviolet radiation. (*a*) Normal dTpT. (*b*) The dT(6–4)T photoproduct with atom numbering.

in accordance with Kabat *et al.*, 1991, and are denoted by the suffixes L and H, respectively).

The (6–4) photoproduct can be repaired by photoreactivation and nucleotide-excision repair. During photoreactivation, a damage-specific enzyme, (6–4) photolyase, recognizes the photoproduct and reverts the damage in a light-dependent reaction, restoring the bases to their native form (Todo *et al.*, 1993; Weber, 2005). Nucleotide-excision repair is a multistep mechanism by which a broad range of DNA lesions including (6–4) photoproducts are repaired. The damage and structural distortion are recognized and excised as a fragment of DNA, and the resulting gap is filled by a DNA polymerase (Gillet & Schärer, 2006). The crystal structure of the DNA (6–4) photolyase in complex with a DNA duplex containing a central (6–4) lesion has revealed that the (6–4) lesion flips out of the DNA duplex into the active site (Maul *et al.*, 2008). A flipped-out (6–4) lesion has also been reported in the crystal structure of the nucleotide-excision repair protein DDB1–DDB2 bound to (6–4)-lesion-containing DNA (Scrima *et al.*, 2008). These structures suggest that recognition of the (6–4) lesion is attained by a structural change of the (6–4)-lesion-containing DNA.

The antibody 64M-5, which exhibits the highest affinity toward the (6–4) photoproduct among the 64M-2, 64M-3 and 64M-5 antibodies, was originally produced against the single-stranded (6–4) DNA (Mori *et al.*, 1991) and was subsequently found to bind the double-stranded (6–4) DNA (Morioka *et al.*, 1998). The structural basis by which 64M-5 can also bind double-stranded (6–4) DNA needs to be investigated. Here, we report the crystal structure of the 64M-5 Fab in complex with a double-stranded DNA containing a T(6–4)T segment. We also discuss the DNA structure and the recognition mechanism of the T(6–4)T segment by comparing the structures of the (6–4) photolyase and the nucleotide-excision repair enzyme.

2. Materials and methods

2.1. Preparation of crystals

Hybridomas producing the 64M-5 and 64M-2 antibodies were kindly provided by Professor O. Nikaido (Kanazawa Gakuin College, Japan). The 64M-2 antibody was purified as reported previously (Yokoyama *et al.*, 2000) and immobilized on a staphylococcal protein A column (Affi-Gel protein A, Bio-Rad) equilibrated with a high-salt phosphate buffer consisting of 10 m*M* NaH_2PO_4, 2 *M* NaCl pH 7.4. Single-stranded DNA (Espec) was dissolved to a concentration of 0.1 m*M* in purified water and irradiated with 254 nm ultraviolet light at 225 kJ m^{-2}. The DNA solution was applied onto the 64M-2–protein A column and washed with the high-salt buffer. The bound (6–4) photoproduct was eluted with the complementary DNA strand. The eluted mixture was incubated at 363 K for 10 min and then slowly cooled to 277 K to form double-stranded DNA.

The 64M-5 antibody Fab was obtained using the method reported for the 64M-2 Fab (Yokoyama *et al.*, 2000). An excess amount of the 64M-5 Fab was added to the double-stranded (6–4) DNA. The mixture was applied onto a DEAE-5PW anion-exchange column (Tosoh) equilibrated with 20 m*M* Tris–HCl pH 7.0 and eluted with a linear gradient from 300 to 500 m*M* NaCl. The major peak of the double-stranded (6–4) DNA in complex with the 64M-5 Fab was collected and concentrated to 80 µ*M* complex in 50 m*M* Tris–HCl, 0.15 *M* NaCl pH 7.2. Crystallization was performed at 277 K by the hanging-drop vapour-diffusion method. The reservoir solution consisted of 12% PEG 3350, 0.1 *M* magnesium acetate, 10 m*M* $[Co(NH_3)_6]Cl_3$, 0.1 *M* Tris–HCl pH 8.0. Droplets were composed of equal volumes (1 µl) of the reservoir and protein–DNA complex solutions.

After gradual addition of PEG 20 000 and 2-propanol as cryoprotectants, plate-shaped crystals were soaked in a reservoir consisting of 24% PEG 20 000, 25% 2-propanol, 50 m*M* magnesium acetate, 15 m*M* $[Co(NH_3)_6]Cl_3$, 50 m*M* Tris–HCl pH 8.0 and flash-cooled at 100 K in a nitrogen-gas stream. These crystals diffracted to 2.5 Å resolution and belonged to space group $P4_32_12$, with unit-cell parameters $a = 68.4$, $c = 243.7$ Å. The asymmetric unit contained one Fab–DNA complex with a V_M value of 2.5 $Å^3$ Da^{-1} and a solvent content of 52%.

2.2. Structure determination and refinement

X-ray diffraction frames were recorded using a MAR165 CCD detector at the BL41XU station of SPring-8, Hyogo, Japan. Diffraction data were collected from one crystal as 154 frames with an oscillation angle of 1.2° and an exposure time of 10 s per frame. Integration and scaling were performed with the programs *DENZO* and *SCALEPACK* (Otwinowski & Minor, 1997). The data-collection statistics are summarized in Table 1.

The crystal structure was determined by the molecular-replacement method using the program *CNS* (Brünger *et al.*,

Table 1
Data-collection and refinement statistics.

Values in parentheses are for the highest resolution shell.

Data collection	
Resolution range (Å)	30.0–2.5 (2.59–2.50)
Wavelength (Å)	0.8000
No. of observed reflections	215015
No. of unique reflections	20541 (1983)
$R_{\rm merge}(I)$†	0.054 (0.240)
Completeness (%)	97.1 (97.2)
Average $I/\sigma(I)$	60.7 (16.0)
Refinement	
R‡/$R_{\rm free}$§	0.247 (0.290)
No. of protein–DNA complexes per asymmetric unit	1
No. of non-H atoms	
Protein	3307
Nucleotide	732
Solvent	151
Average B factors (Å^2)	
Protein	52.5
Nucleotide	73.1
Solvent	40.2
R.m.s. deviations from ideality	
Bond lengths (Å)	0.009
Bond angles (°)	1.420
Main-chain torsion-angle statistics (%)	
Favoured	90.1
Allowed	8.0
Outliers	1.9

† $R_{\rm merge}(I) = \sum_{hkl}\sum_i |I_i(hkl) - \langle I(hkl)\rangle|/\sum_{hkl}\sum_i I_i(hkl)$, where $I_i(hkl)$ is the intensity of an individual reflection and $\langle I(hkl)\rangle$ is the mean intensity of that reflection. ‡ $R = \sum_{hkl}\big||F_{\rm obs}| - |F_{\rm calc}|\big|/\sum_{hkl}|F_{\rm obs}|$, where $|F_{\rm obs}|$ and $|F_{\rm calc}|$ are the observed and calculated structure-factor amplitudes, respectively. § $R_{\rm free}$ is calculated for 10% of the reflections randomly excluded from refinement.

1998). The structure of the 64M-2 Fab was used as a search model. The highest value obtained in a cross-rotation search using data in the resolution range 8–4 Å was 1.8 times larger than the second highest value. This solution was subjected to a translation search and rigid-body refinement. At this stage, the crystallographic R factor was 0.395 for data in the resolution range 8–3.5 Å. After simulated annealing from 3000 to 300 K using data in the resolution range 8–3 Å, the R factor decreased to 0.324 ($R_{\rm free}$ = 0.414). Nucleotides, including the (6–4) photoproduct, were clearly observed in the electron-density maps and were included in the model using *TURBO-FRODO* (Roussel & Cambillau, 1995) and *Coot* (Emsley & Cowtan, 2004).

After cycles of manual rebuilding and simulated-annealing refinement using data in the resolution range 8–2.5 Å, individual B factors were refined. Ordered water molecules observed in electron-density maps were modelled. After these refinements, the R factor decreased to 0.247 ($R_{\rm free}$ = 0.290) using data in the resolution range 30–2.5 Å. The refinement statistics are summarized in Table 1. Accessible surface areas were calculated using *AREAIMOL* in the *CCP*4 suite (Winn *et al.*, 2011). Least-squares fittings of crystal structures were performed with *LSQKAB* in the *CCP*4 suite (Winn *et al.*, 2011). DNA bending was analyzed by the program *Curves+* (Lavery *et al.*, 2009). All molecular figures were produced with *PyMOL* (http://www.pymol.org/). The atomic coordinates and structure factors have been deposited in the RCSB Protein Data Bank with accession code 3vw3.

3. Results and discussion

3.1. Preparation of double-stranded (6–4) DNA in complex with the 64M-5 Fab

To determine the length of the double-stranded (6–4) DNA necessary for the complex to form, we performed gel-filtration analyses of 14 and 18 bp double-stranded (6–4) DNAs in complex with the 64M-5 and 64M-2 Fabs (Supplementary Table S1 and Fig. S1[1]). In the case of the 14 bp double-stranded (6–4) DNA, the 64M-5 or 64M-2 Fab only formed a complex with the T(6–4)T-containing strand by unravelling the complementary strand. Although the 18 bp double-stranded (6–4) DNA did not bind to the 64M-2 Fab, it formed a complex with the 64M-5 Fab, which exhibits an affinity constant at least tenfold higher than 64M-2 (Mori *et al.*, 1991; Kobayashi *et al.*, 1999). Thus, the 18 bp double-stranded (6–4) DNA is sufficient for the complex to form without unravelling all the flanking base pairs. As discussed below, the 64M-5 Fab recognizes the T(6–4)T segment flipped out of the duplex. The nucleotide flipping caused by the binding of Fabs to the 14 bp DNA destabilizes the DNA duplex and results in the dissociation of the complementary DNA strand. As the 18 bp DNA has flanking base pairs longer than those of the 14 bp DNA, the 64M-2 Fab does not cause nucleotide flipping and does not bind the double-stranded (6–4) DNA. The structural differences between 64M-5 and 64M-2 will be discussed later. In contrast, these results suggested that the 18 bp single-stranded (6–4) DNA bound to the 64M-2 Fab can be liberated from the Fab by addition of the complementary strand. Therefore, the 64M-2 antibody is suitable for purification of the double-stranded (6–4) DNA, as described in §2. Ultraviolet light-irradiated single-stranded DNA was applied onto the immobilized 64M-2 antibody–protein A column and the bound single-stranded (6–4) DNA could be eluted with the complementary strand to form a DNA duplex.

In order to crystallize the 64M-5 Fab in complex with the double-stranded (6–4) DNA, DNA with or without overhangs at the 5′-ends of both strands (Supplementary Table S1) was prepared. The 17 bp DNA with overhangs gave crystals that diffracted synchrotron X-rays to 2.5 Å resolution and was used for further analyses.

3.2. Overall structure

The crystal structure of the 64M-5 Fab in complex with the double-stranded (6–4) DNA was determined by molecular replacement. The mean coordinate error was estimated to be 0.28 Å. The statistics of the diffraction data collection and structure refinement are summarized in Table 1. The main-chain torsion angles of the Fab were analyzed using the program *MolProbity* (Chen *et al.*, 2010). 1.9% of the residues were in outlier regions. These contained a glycine and three proline residues, and mostly belonged to the constant regions of the Fab. All six CDR loops were located in continuous

[1] Supplementary material has been deposited in the IUCr electronic archive (Reference: MH5079). Services for accessing this material are described at the back of the journal.

electron density. The root-mean-square (r.m.s.) difference of the main-chain atoms between the 64M-5 and 64M-2 Fabs (Yokoyama *et al.*, 2012) is 0.60 Å for the variable domains, indicating that the main-chain structure of the 64M-5 Fab is virtually identical to that of the 64M-2 Fab.

In the antigen-binding pocket composed of CDR residues, nucleotides A8, T9(6–4)T10 and A11 are observed as distinct electron densities (Fig. 2). The A8 and T9(6–4)T10 nucleotides are in a flipped-out conformation owing to the unravelling of the base pairs. Nucleotide pairs other than the A8 and T9(6–4)T10 nucleotides are in the Watson–Crick base-pairing conformation and are also observed as clear electron density (Fig. 3). The overhang bases at the 5′-end of both strands interact with the other overhangs related by crystallographic symmetry (Supplementary Fig. S2). Therefore, the DNA duplexes are stacked to form a pseudo-continuous helix, as observed in several protein–DNA complexes (Komori *et al.*, 1999; Tan *et al.*, 2000).

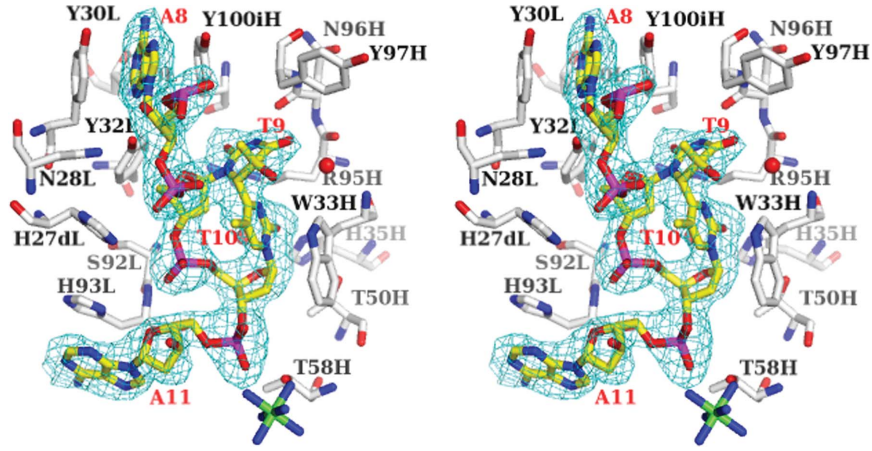

Figure 2
Stereo drawing of the $F_o - F_c$ electron-density map. The map was calculated with phases from the model without the A8, T9(6–4)T10 and A11 nucleotides and is contoured at 3σ. The nucleotides are shown as stick models (C atoms, yellow; N atoms, blue; O atoms, red; P atoms, magenta) and labelled in red. The Fab residues in the vicinity of the four nucleotides are shown as white sticks. Cobalt hexammine is shown as a stick model (with cobalt ions in green). Water molecules are shown as red spheres.

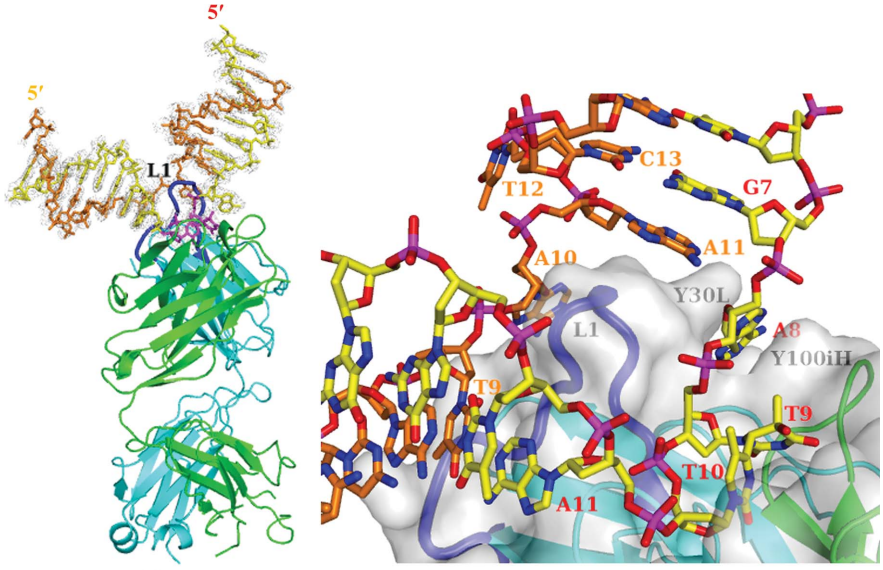

Figure 3
Overall structure of the complex. (*a*) DNA is represented as stick models. The T(6–4)T segment is shown in magenta, the T(6–4)T-containing strand in yellow (the 5′-end is labelled in red) and the complementary strand in orange (the 5′-end is labelled in orange). The $F_o - F_c$ electron-density map is calculated with phases from the model without the double-stranded (6–4) DNA and is contoured at 1.5σ. The heavy chain of Fab is shown in green and the light chain in cyan. The CDR L1 loop inserted between the T(6–4)T-containing strand and the complementary strand is shown in blue. (*b*) Close-up view. The Fab is also represented as a grey surface model. The T(6–4)T-containing strand is labelled in red and the complementary strand in orange.

3.3. DNA–Fab interaction

All six CDRs are involved in DNA recognition. A loop comprised of CDR L1 residues Val27cL, His27dL, Ser27eL, Asn28L, Gly29L and Tyr30L is inserted between the flipped-out T(6–4)T-containing strand and the complementary DNA strand (Figs. 3 and 4). The loop insertion can occur concomitantly with the flipping of the DNA strands. Specific and extensive recognition of the photoproduct can be achieved by this separation. The separation of strands by loop insertion has also been suggested for the nucleotide-excision repair protein UvrB (Truglio *et al.*, 2006). The surface area of DNA interfaced with Fab is 1052 Å^2. Most of this large area is ascribable to the A8, T9(6–4)T10 and A11 nucleotides (674 Å^2) and also to the complementary T9, A10 and A11 (352 Å^2). The T9(6–4)T10 segment is accommodated in the antigen-binding pocket, as shown in Fig. 4. The side chains of His35H and Arg95H are located at the bottom of the pocket. Hydrogen bonds are formed between the Arg95H N$^{\varepsilon}$ and T9 O2 atoms (with a distance of 2.8 Å), between the Arg95H N$^{\eta 2}$ and T9 O2 atoms (2.9 Å) and between the His35H N$^{\varepsilon 2}$ and T10 O2 atoms (2.8 Å). A water molecule is hydrogen bonded to the T10 O2 and Gly91L O atoms. His27dL and His93L are located at the side wall. These basic side chains make electrostatic interactions with the phosphate group of the T9(6–4)T10 segment. The O1P atom of the phosphate group connecting T9 and A10 is hydrogen bonded to the His93L N atom (2.5 Å). The side chains of Trp33H, Tyr97H and Tyr100iH form the side wall of the pocket and show van der Waals interactions with base moieties of the T9(6–4)T10 segment. A water molecule is hydrogen bonded to the T9 O4, Arg95H O and Trp33H N atoms. The N3 atom of

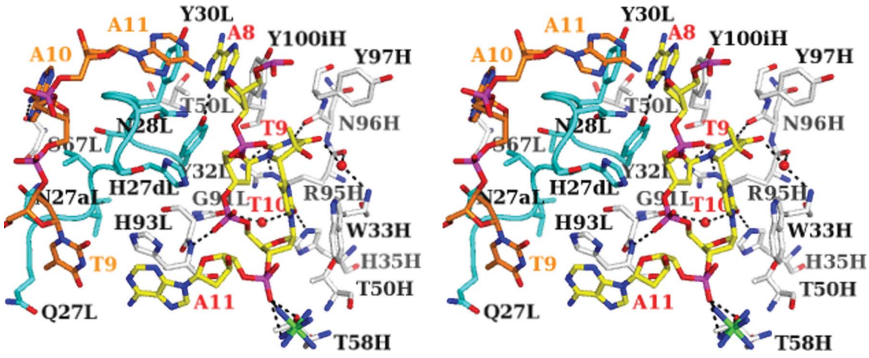

Figure 4
Stereo drawing of the antigen-binding site. The L1 loop is shown in cyan, with the side chains represented as stick models. Hydrogen bonds are shown as broken lines. The T9(6–4)T10 segment and the adjacent A8 base are accommodated in the binding pocket.

the T9 base is hydrogen bonded to the Asn96H O atom (3.1 Å). The A8 base is sandwiched by the side chains of Tyr30L and Tyr100iH. The N3 atom of the A8 base is hydrogen bonded to the Tyr32L O^{η} atom (2.6 Å). The His93L side chain interacts with the A11–T9 base pair in a stacking manner. The O2P atom of the phosphate group connecting T10 and A11 is hydrogen bonded to the Thr58H $O^{\gamma 1}$ atom (2.5 Å). Electron density corresponding to the cobalt hexammine used for crystallization was observed in the vicinity of this phosphate group. Two N atoms of the cobalt hexammine are hydrogen bonded to the O2P atom of this phosphate group.

No hydrogen bonds are observed between the complementary DNA strand and the CDR L1 residues. The nucleotides A10 and A11 in the complementary strand are located along the side of the CDR L1 loop. The surface area of these nucleotides interfaced with Fab is 216 $Å^2$. The A10 adenine base is flipped-out of the duplex and the A10 N6 is hydrogen bonded to the Ser67L O^{γ} atom (2.9 Å). The A10 base interacts with the symmetry-related A10 base in a stacking manner.

3.4. Comparison between 64M-5 and 64M-2 Fabs

The 64M-5 antibody exhibits an affinity constant K_d of 2.2×10^{-7} *M* for the dT(6–4)T ligand (Kobayashi *et al.*, 1998). This affinity is at least an order of magnitude higher than that of 64M-2. The residues His27dL, Asn28L, Tyr32L, Gly91L, Trp33H, His35H, Arg95H and Tyr100iH are identical in the two antibodies and show almost the same conformation (Fig. 4, Supplementary Fig. S3). The surface area of the 64M-5 Fab interfaced with the T9(6–4)T10 nucleotides without the T9 phosphate is 296 $Å^2$. The value is comparable with the buried area of 291 $Å^2$ for the 64M-2 Fab in complex with dT(6–4)T (Yokoyama *et al.*, 2000). On comparing the binding of dT(6–4)T to these two antibodies, differences were mainly observed for residues 93L and 97H (Supplementary Fig. S3). The His93L side chain exhibits electrostatic interactions with the phosphate group of dT(6–4)T. In 64M-2, His93L is replaced by the neutral residue Leu. The Tyr97H side chain of 64M-5 shows van der Waals interaction with the T9 base. In 64M-2, Tyr97H is replaced by Gly. The replacement of these residues in the 64M-2 antibody gives rise to a loss of electrostatic and van der Waals interactions responsible for the higher affinity of 64M-5 for the dT(6–4)T ligand.

The surface area of the 64M-5 Fab interfaced with the tetranucleotide A8, T9(6–4)T10 and A11 without the A8 phosphate is 549 $Å^2$. The value is larger than the buried area of 487 $Å^2$ for the 64M-2 Fab in complex with dTT(6–4)TT (Yokoyama *et al.*, 2012), although the flanking nucleotides differ between 64M-5 Fab–dAT(6–4)TA and 64M-2 Fab–dTT(6–4)TT. On comparing the binding of the tetranucleotides containing the central T(6–4)T segment between the two antibodies, major differences were found at residues 30L and 93L (Supplementary Fig. S3). The aromatic side chains of Tyr30L and His93L are located parallel to the flanking A8 and A11 bases, respectively. The buried surface area of Tyr30L of 64M-5 is 35.6 $Å^2$ larger than that of Asn30L of 64M-2. The buried area of His93L of 64M-5 is 41.0 $Å^2$ larger than that of Leu93L of 64M-2. These interactions cause the higher affinity of 64M-5 for the tetranucleotide compared with that of 64M-2. In the 64M-2 Fab in complex with dTT(6–4)TT the Lys50L side chain makes electrostatic interactions with the 5′-terminal T1 base (Supplementary Fig. S3; Yokoyama *et al.*, 2012). If the 64M-2 Fab interacts with dAT(6–4)TA, the Lys50L side chain of 64M-2 would cause steric hindrance with the 5′-terminal adenine base. Thus, Thr50L of 64M-5 is suitable for binding dAT(6–4)TA.

The 64M-5 Fab forms a complex with the double-stranded (6–4) DNA, but the 64M-2 Fab does not. The CDR L1 residues are almost the same in 64M-5 and 64M-2 except for residues 27aL and 30L (Supplementary Fig. S3*b*). The L1 residues make van der Waals interactions with the complementary strand and form no hydrogen bonds. The larger side chain of Asn27aL (64M-5) compared with Ser27aL (64M-2) makes van der Waals interactions with the complementary strand, partly contributing to the increased affinity of 64M-5 compared with 64M-2. In 64M-5, the side chains of Tyr30L and His93L are stacked with the flanking A8 and A11 bases, respectively, and therefore the 64M-5 Fab can bind the flipped-out T(6–4)T-containing nucleotides even in the presence of the flanking base pairs and forms a stable complex with the double-stranded (6–4) DNA. In 64M-2, Asn30L and Leu93L interact with the A8 and A11 bases, respectively, more weakly than in 64M-5, and Lys50L causes steric hindrance with the A8 base (Supplementary Fig. S3). The 64M-2 Fab does not cause nucleotide flipping owing to its weak interactions with the T(6–4)T-containing nucleotides in the presence of robust flanking base pairs and therefore does not bind the double-stranded (6–4) DNA.

3.5. DNA structure

A schematic diagram of the double-stranded DNA in complex with the 64M-5 Fab is shown in Fig. 5. Nucleotide

Table 2
DNA torsion angles.

	Torsion angle (°)								
	T(6–4)T-containing strand				Complementary strand				
Torsion definition	A8	T9†	T10†	A11	T9	A10	A11	T12	B-DNA‡
Glycosidic linkage									
χ§	−157	−109	−60	−81	−96	−104	−175	−64	−117
Backbone									
α (O3′—P—O5′—C5′)	141	−42	−89	−62	−32	−75	−60	52	−63
β (P—O5′—C5′—C4′)	158	179	−140	−127	−179	−121	141	−171	171
γ (O5′—C5′—C4′—C3′)	−161	41	24	16	42	49	−76	59	54
δ (C5′—C4′—C3′—O3′)	140	107	121	148	148	144	138	141	123
ε (C4′—C3′—O3′—P)	−129	−150	−155	177	−105	−131	−122	−164	−169
ζ (C3′—O3′—P—O5′)	−93	−64	85	−131	−115	169	102	49	−108

† T9 and T10 represent the two thymidines of the T(6–4)T segment in the double-stranded (6–4) DNA in complex with the 64M-5 Fab. ‡ The mean torsion angles of a double-stranded B-DNA, the so-called Drew–Dickerson dodecamer (Drew *et al.*, 1981), are also shown. § The torsion angle χ is the angle O4′—C1′—N1—C2 for T and O4′—C1′—N9—C4 for A.

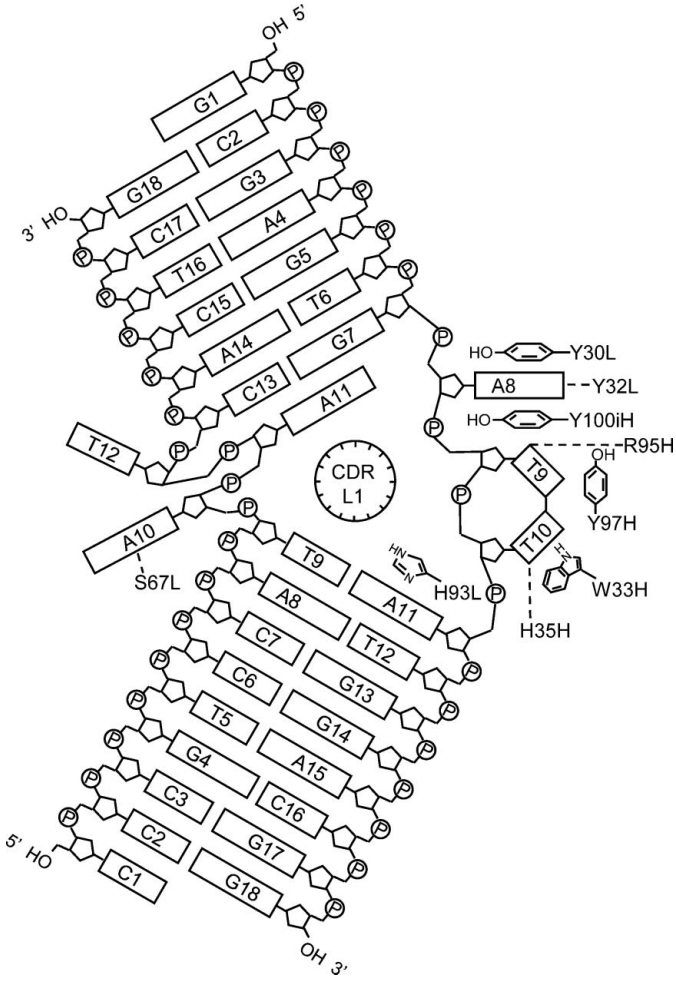

Figure 5
Schematic representation of the DNA structure. A8 and T9(6–4)T10 of the T(6–4)T-containing strand and A10 and T12 of the complementary strand are flipped out of the duplex. Fab residues that make van der Waals interactions are indicated by side-chain models. Hydrogen bonds are shown as broken lines. The CDR L1 loop inserted between the strands is shown as a circle with hatched lines.

pairs C2–G18 to G7–C13 form a B-DNA duplex. The A8 and complementary T12 nucleotides are flipped out of the duplex (Fig. 3*b*). The A8 adenine base is involved in interactions with the side chains of Tyr30L and Tyr100iH of the Fab. The photoproduct T9(6–4)T10 is accommodated in a concave pocket of the Fab molecule. The complementary A11 interacts with the G7–C13 base pair in a stacking manner. The nucleotide pairs A11–T9 to G18–C2 form another B-DNA duplex. The DNA helices flanking the T(6–4)T segment are kinked by 87°.

The T9(6–4)T10 segment in a closed circular structure has a small r.m.s. difference of 0.34 Å from that of the dT(6–4)T structure in complex with the 64M-2 Fab (Yokoyama *et al.*, 2000), indicating that the dT(6–4)T structure is not affected by the flanking nucleotides. The T9 base is in the half-chair conformation and the T10 base is in the planar conformation. The six-membered ring planes of the T9 and T10 bases are nearly perpendicular, with an interplanar angle of 80°. The torsion angles for the A8, T9(6–4)T10 and A11 nucleotides and the complementary T9, A10, A11 and T12 nucleotides are summarized in Table 2. The torsion angles of the standard double-stranded B-DNA (Drew *et al.*, 1981) are also given in this table for comparison. The glycosidic torsion angle χ of most nucleotides is in the *anti* range (Saenger, 1984), while that of T10 of the T(6–4)T segment is in the *high-anti* range, as observed in the 64M-2 Fab structure (Yokoyama *et al.*, 2000, 2012). The glycosidic torsion angle χ of T12 of the complementary strand is also in the *high-anti* range because the complementary T12 base is exposed to the solvent and is slightly distorted by interaction with the symmetry-related Fab residues. The torsion angle γ, which describes the direction of the O5′ atoms relative to the C4′—C5′ bonds (the atom numbering used refers to Fig. 1), is almost in the *gauche*$^+$ range, except for A8 of the T(6–4)T-containing strand and A11 of the complementary strand. The ζ and α torsion angles of the phosphodiester bonds are in the *gauche*$^-$ range, except for the A8 α and T10 ζ torsion angles of the T(6–4)T strand and the A10 ζ, A11 ζ, T12 α and T12 ζ torsion angles of the complementary strand. The A8 and T9(6–4)T10 nucleotides are flipped out of the duplex and thus the A8 α and A10 ζ torsion angles next to the trinucleotide A8–T9–T10 are in an unusual range. The complementary A10 and T12 nucleotides are also flipped out of the duplex and thus the T12 α, A10 ζ, A11 ζ and A12 ζ torsion angles next to the A10 and T12 nucleotides are in an unusual range. If the ζ angle of T10 of the T(6–4)T strand is in the *gauche*$^-$ range, the A11 deoxyribose would be directed toward the CDR H2 residues, resulting in steric hindrance with Asp56H and Thr58H (Fig. 4).

The DNA structure in complex with the 64M-5 Fab is kinked by 87° at the T(6–4)T segment (Fig. 6*a*). The T(6–4)T segment is flipped out of the duplex and directly recognized by

the 64M-5 Fab. The complementary strand makes a number of interactions with light-chain residues, including those of the inserted L1 loop. The T(6–4)T segment is set apart from the complementary strand with these interactions, giving rise to the 87° kink at the photolesion. In the solution structure of uncomplexed double-stranded DNA containing dT(6–4)T and complementary AA nucleotides, the (6–4) photoproduct retains Watson–Crick base pairing throughout the duplex, except at the 3′-side of the T(6–4)T lesion, leading to a rather moderate 44° bending in the overall DNA duplex (Kim & Choi, 1995). In the other solution structure of uncomplexed double-stranded DNA containing dT(6–4)T and complementary GA nucleotides, the 5′-side and 3′-side (6–4) bases are hydrogen bonded to the adenine and guanine bases, respectively, leading to a 27° bending in the overall DNA duplex (Lee *et al.*, 1999). Therefore, the intensive interaction with the CDR loops of the 64M-5 antibody should account for the steep kink and resultant strand separation. This suggests that even in double-stranded DNA the (6–4) photoproduct can be detected using the 64M-5 antibody.

3.6. Structural comparison with repair enzymes

The (6–4) photoproduct can be repaired by photoreactivation and nucleotide-excision repair. Photoreactivation is

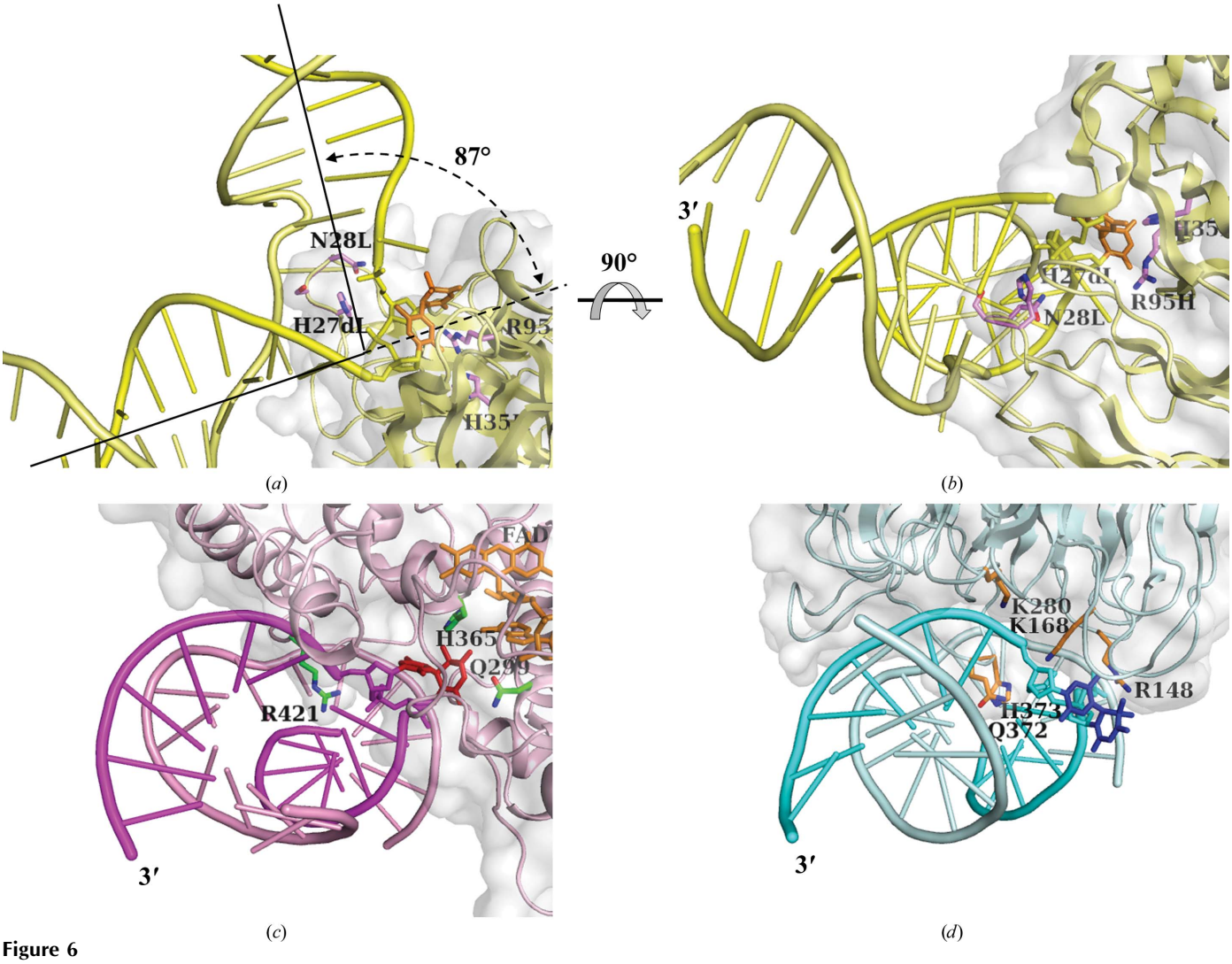

Figure 6
Comparison of double-stranded (6–4) DNA in complex with the 64M-5 Fab, the (6–4) photolyase and the nucleotide-excision repair protein DDB1–DDB2. DNA and proteins are represented as cartoon models and the T(6–4)T segments and some residues involved in interaction with the T(6–4)T segments are shown as stick models. Proteins are also represented as grey surface models. The complementary strand is shown in a paler colour than the T(6–4)T-containing strand. The 3′-end of the T(6–4)T-containing strand is labelled 3′. (*a*) The double-stranded (6–4) DNA in complex with the 64M-5 Fab is shown in yellow. The overall bend of the DNA duplex is 87°. The base moiety of the T(6–4)T segment is shown in orange. (*b*) The same structure as in (*a*), viewed from the 3′-end of the T(6–4)T-containing strand. The view is almost the same as in (*c*) and (*d*) if the T(6–4)T-containing strands are superposed between the 64M-5 Fab, (6–4) photolyase and DDB1–DDB2 protein structures. (*c*) The double-standed (6–4) DNA in complex with the (6–4) photolyase (PDB entry 3cvu; Maul *et al.*, 2008) is shown in magenta and viewed from the 3′-end of the T(6–4)T-containing strand. The base moiety of the T(6–4)T segment is shown in red. FAD is shown in orange. (*d*) The double-standed (6–4) DNA in complex with DDB1–DDB2 protein (PDB entry 3ei1; Scrima *et al.*, 2008) is shown in cyan and viewed from the 3′-end of the T(6–4)T-containing strand. The base moiety of the T(6–4)T segment is shown in blue.

performed by a damage-specific (6–4) photolyase which binds to the photoproduct and repairs the damage in a light-dependent reaction. The structure of the double-stranded (6–4) DNA in complex with the 64M-5 Fab can be compared with those of the double-stranded (6–4) DNA in complex with the (6–4) photolyase and the nucleotide-excision repair protein DDB1–DDB2. Figs. 6(*b*), 6(*c*) and 6(*d*) show the photoproduct-binding sites of these structures, in which the T(6–4)T-containing strands are superposed.

As shown in Fig. 6(*c*), the (6–4) photolyase recognizes the T(6–4)T segment completely flipped out of the duplex. The 5′-thymine base of the T(6–4)T segment is hydrogen bonded to the side chains of Gln299 and His365, while no hydrogen bonds are observed for the 3′-pyrimidone base (Maul *et al.*, 2008). The hydrophobic residues Pro247, Pro293, Val294, Trp302 and Trp409 form a side wall of the pocket and interact with the T(6–4)T bases. The Arg421 side chain protrudes into the duplex and contributes to the setting apart of the T(6–4)T segment. In the 64M-5 Fab, the side chains of Arg95H and His35H are hydrogen bonded to the 5′-thymine and 3′-pyrimidone bases of the T(6–4)T segment, respectively (Figs. 6*a* and 6*b*). A major similarity between the 64M-5 Fab and (6–4) photolyase structures is that the 5′-thymine base is recognized by hydrogen-bonding and aromatic–aromatic interactions. Differences are observed in the orientation of the recognition of the T(6–4)T segment. The 64M-5 Fab recognizes the T(6–4)T bases along with the sugar-phosphate backbone. In the (6–4) photolyase the base moiety of the T(6–4)T segment is plunged into the binding pocket and the sugar-phosphate moiety is left on the surface of the pocket. This is because the (6–4) photolyase converts the (6–4) linked base into a normal TT base by transferring electrons from FAD located inside the protein (Fig. 6*c*).

The nucleotide-excision repair enzyme first excises and removes a short stretch of DNA containing the damaged base (Gillet & Schärer, 2006). In the nucleotide-excision repair protein DDB1–DDB2 (Fig. 6*d*), the side chains of Arg148, Lys168 and Lys280 show electrostatic interactions with the phosphate groups around the T(6–4)T segment and no hydrogen bonds are observed in the T(6–4)T bases (Scrima *et al.*, 2008). The hydrophobic residues Pro191, Ile213, Trp236 and Trp239 form a shallow pocket and interact with the T(6–4)T bases. The side chains of Gln372 and His373 forming a turn are inserted into the duplex and interact with the complementary AA nucleotides as substitutes for the flipped-out T(6–4)T segment and thus contribute to the flipping of the T(6–4)T segment. Major similarities between the 64M-5 Fab and DDB1–DDB2 structures are that the T(6–4)T bases are recognized by aromatic–aromatic interactions and that large loops are inserted into the duplexes. However, the face of the T(6–4)T segment recognized by the DDB1–DDB2 protein is diametrically opposite to that recognized by the 64M-5 Fab. In DDB1–DDB2, the sugar-phosphate moiety of the T(6–4)T segment is oriented towards the surface of the binding pocket, while the base moiety is rather exposed to the solvent. This orientation is appropriate for the excision repair of the nucleotides in which the phosphodiester bond in the sugar-phosphate moiety is excised.

In the (6–4) photolyase and DDB1–DDB2 structures, two nucleotides of T(6–4)T are flipped out of the duplex and all of the remaining nucleotides retains Watson–Crick base pairing throughout the duplex (Maul *et al.*, 2008; Scrima *et al.*, 2008). The DNA-bending angles are 48° for (6–4) photolyase and 34° for DDB1–DDB2. In the 64M-5 Fab, on the other hand, three nucleotides, A8 and T9(6–4)T10, are flipped out of the duplex and are stabilized by interactions between the A8 base and the side chains of Tyr30L and Tyr100iH and between the A11 base and the His93L side chain (Figs. 4 and 5). The CDR L1 loop including His27dL and Asn28L is inserted into the duplex as described above, resulting in a DNA kink angle of 87° (Fig. 6*a*). The antibodies 64M-2, 64M-3 and 64M-5 were originally produced against the single-stranded (6–4) DNA (Mori *et al.*, 1991). However, the 64M-5 Fab also binds the double-stranded (6–4) DNA by partly separating the double strand. Thus, the antibody 64M-5 is suitable for the detection of both single-stranded and double-stranded (6–4) DNA. The structure determined here provides a clue for the production of antibodies with improved affinity for the photoproduct.

The structural comparison of these protein structures in complex with the double-stranded (6–4) DNA indicates that the antibody 64M-5, the photoreactivation enzyme (6–4) photolyase and the nucleotide-excision repair protein DDB1–DDB2 have distinctive binding-site structures that are appropriate for their functions. However, in all of these complex structures the T(6–4)T segment is flipped out of the duplex and the DNA helices are kinked at the photolesion. Since bendings of 44° and 27° were also observed in the solution structures of uncomplexed double-stranded DNA containing the (6–4) photoproduct (Kim & Choi, 1995; Lee *et al.*, 1999), the covalent link in the (6–4) photolesion accounts for the kink in the double-stranded DNA. The steeper kink observed for the 64M-5 structure can be ascribed to the intensive interaction between the complementary strand and CDR residues. Although the T(6–4)T segments in the solution structures were not flipped out but were partly hydrogen bonded to the complementary strand (Kim & Choi, 1995; Lee *et al.*, 1999), the flipping out is common to the crystal structures of 64M-5 Fab, (6–4) photolyase and DDB1–DDB2. This indicates that the flipped-out structure is one of the possible conformations of double-stranded (6–4) DNAs. As discussed in Scrima *et al.* (2008), the double-stranded (6–4) DNA shows diminished intrastrand stacking and interstrand hydrogen-bonding interactions around the lesion, allowing the insertion of the hairpin loop and the flipping out of the T(6–4)T segment. In the absence of the lesion, however, the intact base stacking and hydrogen-bonding interactions would represent an energy barrier that precludes the insertion of the hairpin loop. The T(6–4)T segment destabilizes the double-stranded DNA structure, leading to an increased propensity of the lesion to flip out. This flipped-out conformation rather than the base-paired conformation is appropriate for recognition by proteins. The structural similarities of the double-stranded (6–4) DNAs in complex with proteins suggest that the flipping

out and kinking of the DNA are common features of mutagenic (6–4) photoproducts recognized by proteins.

We thank Professor O. Nikaido (Kanazawa Gakuin College, Japan) for kindly providing us with the hybridomas producing the 64M-5 and 64M-2 antibodies. We thank the SPring-8 staff for assistance with data collection. This work was supported by a Grant-in-Aid for Specially Promoted Research (No. 08101001 to YS) and also by a Grant-in-Aid for Young Scientists (B) (No. 21770122 to HY) from the Ministry of Education, Culture, Sports, Science and Technology of Japan.

References

Brünger, A. T., Adams, P. D., Clore, G. M., DeLano, W. L., Gros, P., Grosse-Kunstleve, R. W., Jiang, J.-S., Kuszewski, J., Nilges, M., Pannu, N. S., Read, R. J., Rice, L. M., Simonson, T. & Warren, G. L. (1998). *Acta Cryst.* D**54**, 905–921.

Chen, V. B., Arendall, W. B., Headd, J. J., Keedy, D. A., Immormino, R. M., Kapral, G. J., Murray, L. W., Richardson, J. S. & Richardson, D. C. (2010). *Acta Cryst.* D**66**, 12–21.

Drew, H. R., Wing, R. M., Takano, T., Broka, C., Tanaka, S., Itakura, K. & Dickerson, R. E. (1981). *Proc. Natl Acad. Sci. USA*, **78**, 2179–2183.

Emsley, P. & Cowtan, K. (2004). *Acta Cryst.* D**60**, 2126–2132.

Gillet, L. C. & Schärer, O. D. (2006). *Chem. Rev.* **106**, 253–276.

Kabat, E. A., Wu, T. T., Perry, H. M., Gottesman, K. S. & Foeller, C. (1991). *Sequences of Proteins of Immunological Interest*, 5th ed. Bethesda: National Institutes of Health.

Kim, J.-K. & Choi, B.-S. (1995). *Eur. J. Biochem.* **228**, 849–854.

Kobayashi, H., Morioka, H., Tobisawa, K., Torizawa, T., Kato, K., Shimada, I., Nikaido, O., Stewart, J. D. & Ohtsuka, E. (1999). *Biochemistry*, **38**, 532–539.

Kobayashi, H., Morioka, H., Torizawa, T., Kato, K., Shimada, I., Nikaido, O. & Ohtsuka, E. (1998). *J. Biochem.* **123**, 182–188.

Komori, H., Sasai, N., Matsunaga, F., Wada, C. & Miki, K. (1999). *J. Biochem.* **125**, 24–26.

Lavery, R., Moakher, M., Maddocks, J. H., Petkeviciute, D. & Zakrzewska, K. (2009). *Nucleic Acids Res.* **37**, 5917–5929.

LeClerc, J. E., Borden, A. & Lawrence, C. W. (1991). *Proc. Natl Acad. Sci. USA*, **88**, 9685–9689.

Lee, J.-H., Hwang, G.-S. & Choi, B.-S. (1999). *Proc. Natl Acad. Sci. USA*, **96**, 6632–6636.

Lindahl, T. (1993). *Nature (London)*, **362**, 709–715.

Maul, M. J., Barends, T. R. M., Glas, A. F., Cryle, M. J., Domratcheva, T., Schneider, S., Schlichting, I. & Carell, T. (2008). *Angew. Chem. Int. Ed.* **47**, 10076–10080.

Mori, T., Nakane, M., Hattori, T., Matsunaga, T., Ihara, M. & Nikaido, O. (1991). *Photochem. Photobiol.* **54**, 225–232.

Morioka, H., Miura, H., Kobayashi, H., Koizumi, T., Fujii, K., Asano, K., Matsunaga, T., Nikaido, O., Stewart, J. D. & Ohtsuka, E. (1998). *Biochim. Biophys. Acta*, **1385**, 17–32.

Otwinowski, Z. & Minor, W. (1997). *Methods Enzymol.* **276**, 307–326.

Roussel, A. & Cambillau, C. (1995). *TURBO-FRODO* v.5.4. Faculté de Médecine Nord, Marseille, France.

Saenger, W. (1984). *Principles of Nucleic Acid Structure*, pp. 14–24. New York: Springer-Verlag.

Scrima, A., Konícková, R., Czyzewski, B. K., Kawasaki, Y., Jeffrey, P. D., Groisman, R., Nakatani, Y., Iwai, S., Pavletich, N. P. & Thomä, N. H. (2008). *Cell*, **135**, 1213–1223.

Tan, S., Hunziker, Y., Pellegrini, L. & Richmond, T. J. (2000). *J. Mol. Biol.* **297**, 947–959.

Todo, T., Takemori, H., Ryo, H., Ihara, M., Matsunaga, T., Nikaido, O., Sato, K. & Nomura, T. (1993). *Nature (London)*, **361**, 371–374.

Truglio, J. J., Karakas, E., Rhau, B., Wang, H., DellaVecchia, M. J., Van Houten, B. & Kisker, C. (2006). *Nature Struct. Mol. Biol.* **13**, 360–364.

Weber, S. (2005). *Biochim. Biophys. Acta*, **1707**, 1–23.

Winn, M. D. *et al.* (2011). *Acta Cryst.* D**67**, 235–242.

Yokoyama, H., Mizutani, R., Satow, Y., Komatsu, Y., Ohtsuka, E. & Nikaido, O. (2000). *J. Mol. Biol.* **299**, 711–723.

Yokoyama, H., Mizutani, R., Satow, Y., Sato, K., Komatsu, Y., Ohtsuka, E. & Nikaido, O. (2012). *Acta Cryst.* D**68**, 232–238.